OXFORD

SOT | Society of Toxicology
academic.oup.com/toxsci

TOXICOLOGICAL SCIENCES, 178(2), 2020, 375–390

doi: 10.1093/toxsci/kfaa146
Advance Access Publication Date: 25 September 2020
Research Article



# Tobacco Smoke Exposure Exacerbated Crystalline Silica-Induced Lung Toxicity in Rats

Tina M. Sager, Christina M. Umbright, Gul Mehnaz Mustafa, Naveena Yanamala, Howard D. Leonard, Walter G. McKinney, Michael L. Kashon, and Pius Joseph[1]

Health Effects Laboratory Division, National Institute for Occupational Safety and Health (NIOSH), Morgantown, West Virginia 26505

[1]To whom correspondence should be addressed at Toxicology and Molecular Biology Branch, National Institute for Occupational Safety and Health, 1095 Willowdale Road, Morgantown, WV 26505. E-mail: pcj5@cdc.gov.

**Disclaimer:** The findings and conclusions in this report are those of the authors and do not necessarily represent the official position of the National Institute for Occupational Safety and Health, Centers for Disease Control and Prevention.

The Next-Generation Sequence data discussed in this publication have been deposited in NCBI's Gene Expression Omnibus (GEO) and are accessible through GEO Series accession number GSE136945.

## ABSTRACT

Smoking may modify the lung response to silica exposure including cancer and silicosis. Nevertheless, the precise role of exposure to tobacco smoke (TS) on the lung response to crystalline silica (CS) exposure and the underlying mechanisms need further clarification. The objectives of the present study were to determine the role of TS on lung response to CS exposure and the underlying mechanism(s). Male Fischer 344 rats were exposed by inhalation to air, CS (15 mg/m$^3$, 6 h/day, 5 days), TS (80 mg/m$^3$, 3 h/day, twice weekly, 6 months), or CS (15 mg/m$^3$, 6 h/day, 5 days) followed by TS (80 mg/m$^3$, 3 h/day, twice weekly, 6 months). The rats were euthanized 6 months and 3 weeks following initiation of the first exposure and the lung response was assessed. Silica exposure resulted in significant lung toxicity as evidenced by lung histological changes, enhanced neutrophil infiltration, increased lactate dehydrogenase levels, enhanced oxidant production, and increased cytokine levels. The TS exposure alone had only a minimal effect on these toxicity parameters. However, the combined exposure to TS and CS exacerbated the lung response, compared with TS or CS exposure alone. Global gene expression changes in the lungs correlated with the lung toxicity severity. Bioinformatic analysis of the gene expression data demonstrated significant enrichment in functions, pathways, and networks relevant to the response to CS exposure which correlated with the lung toxicity detected. Collectively our data demonstrated an exacerbation of CS-induced lung toxicity by TS exposure and the molecular mechanisms underlying the exacerbated toxicity.

**Key words:** tobacco smoke; crystalline silica; lung toxicity; mechanisms; gene expression.

Exposure to silica is almost unavoidable because of its natural occurrence and rich abundance in earth's crust. However, the most significant exposure to crystalline silica (CS)—the more toxic form of silica—occurs in specific tasks such as mining, construction, tunneling, sand blasting, silica milling, and hydraulic fracturing. The National Institute for Occupational Safety and Health (NIOSH) recommended exposure limit (REL) and the Occupational Safety and Health Administration (OSHA) permissible exposure limit (PEL) for CS is 50 μg/m$^3$ per day (National Institute for Occupational Safety and Health, 1996;

Occupational Safety and Health Administration, 2013). However, occupational exposure to CS as high as 10 times the NIOSH REL or OSHA PEL has been reported (Doney *et al.*, 2020).

Inhalation exposure to CS at levels exceeding the NIOSH REL or OSHA PEL may result in adverse health effects among the exposed workers. The most serious health effects associated with occupational exposure to CS are those affecting the pulmonary system. Based on the results obtained from animal and human studies, the International Agency for Research on Cancer (IARC) has classified CS as a human carcinogen (IARC, 1997). Another major adverse health effect potentially associated with excess occupational exposure to CS is silicosis—an irreversible, progressive, and potentially fatal obstructive pulmonary pneumoconiosis (Greenberg *et al.*, 2007). Despite the progress made in the prevention of silicosis over the past few decades, morbidity and mortality associated with silicosis continues to be a problem in the United States (U.S. Department of Health and Human Services, 2008). Both the International Labor Organization and the World Health Organization are seriously concerned about the large number of deaths associated with occupational exposure to CS, especially in developing countries.

The pulmonary response to CS and the associated adverse health effects may be modified by multiple factors, most notably gene polymorphisms and cigarette smoking. Yucesoy *et al.* (2001), based on the results obtained from a case-control study involving male Caucasian underground miners (325 cases and 164 controls), found a strong association between silicosis incidence and polymorphisms of the TNF-α gene. Similarly, based on the results of a meta-analysis involving 1990 silicosis and 1898 healthy controls, Zhang *et al.* (2019) concluded that TNF-α polymorphisms are associated with susceptibility to silicosis. Nevertheless, contrary to the findings of these reports, there are studies that failed to demonstrate an association between silicosis and TNF-α polymorphisms (Qu *et al.*, 2007; Wu *et al.*, 2008). Another factor that has been studied extensively with respect to its role in modifying the pulmonary response to CS, especially lung cancer and silicosis, is cigarette smoking. The carcinogenic potential of CS has been the subject of many animal and human studies. Overall, these studies suggested an association between exposure to CS and an increased risk for lung cancer justifying the classification of CS as a human carcinogen (IARC, 1997). However, the findings of many of the human studies linking CS exposure and cancer outcome are difficult to interpret because they do not correctly consider the contribution by coexposure to tobacco smoke (TS), another known human carcinogen (IARC, 2004). Hessel *et al.* (2003) reviewed the evidence gathered from 13 human studies with respect to the role of TS exposure on silicosis and concluded that more studies were needed to precisely determine the relationship between silicosis and smoking. Of the 13 studies reviewed, 3 supported a positive involvement of smoking in silicosis, whereas 8 provided only limited support. Although one study did not support a role for smoking on silicosis, the findings of another study suggested an inverse relationship between smoking and silicosis. The controversial role of cigarette smoking on the health effects associated with CS exposure is further illustrated by the results obtained from a study in which the joint effects of smoking and CS exposure on lung diseases [cancer, chronic obstructive pulmonary disease (COPD), silicosis, and tuberculosis] were investigated in a cohort consisting of over 3000 silicosis cases (Tse *et al.*, 2014). The findings of the study differed considerably depending on whether the data are corrected for "smoking adjustment factors (SAFs)." The standardized mortality ratio calculated when SAFs were not taken into consideration were biased and higher for cancer, COPD, silicosis, and tuberculosis among smokers compared with never smokers. However, the SAFs-corrected standardized mortality ratio for lung cancer, COPD, and silicosis was lower among CS-exposed smokers compared with never smokers. The SAF-corrected independent risk ratio effect of CS exposure on the lung diseases such as cancer, COPD, and silicosis was 81%–95% of that among never smokers. Tuberculosis associated with CS exposure among smokers, on the other hand, was 21% higher than that in never smokers. In addition to gene polymorphisms and cigarette smoking, coexposure to toxicants such as arsenic, radon, and polycyclic aromatic hydrocarbons has been shown to modify the pulmonary response to CS exposure in human subjects (Cocco *et al.*, 2001).

The presence of confounders or modifiers of CS toxicity, which are very difficult to control in a human study, makes it difficult to interpret the findings of human studies investigating the adverse health effects associated with CS exposure. On the other hand, in animal studies, the presence of modifiers of toxicity can be easily controlled which enables the precise linking of the toxicity detected, if any, to CS and/or the modifier(s). The objectives of the current rat inhalation toxicity study were (1) to determine precisely whether TS exposure modifies CS-induced pulmonary toxicity and (2) to determine the molecular mechanisms underlying the modification, if any, of CS-induced pulmonary toxicity by TS exposure.

## MATERIALS AND METHODS

*Animals.* Approximately 3 months old, pathogen-free, and healthy male Fischer 344 rats (CDF strain) purchased from Charles River Laboratories (Wilmington, Massachusetts) were used in this study. The entire animal study was conducted in an AAALAC International accredited animal facility (NIOSH, Morgantown, WV) following a protocol approved by the Institutional Animal Care and Use Committee. The rats, upon their arrival, were acclimated to the animal facility conditions for 12 days prior to their use in the study. Throughout the entire period of the study, the rats were housed in groups of 3 rats/cage and maintained on a 12-h light-dark cycle in a temperature (68°F–72°F) and humidity (30%–70%) controlled room. Food and water were provided *ad libitum* except when the rats were exposed by inhalation to the agents as described below.

*Silica aerosol generation.* An aerosol containing Min-U-Sil5 CS (US Silica, Berkley Springs, West Virginia) was generated using the same system and procedure employed in our previous study (Sellamuthu *et al.*, 2011).

*Tobacco smoke aerosol generation.* The 3R4F reference cigarette (University of Kentucky Tobacco Research and Development Center, Lexington, Kentucky) was used in this study. The cigarettes were stored at 70°F and 60% relative humidity in a humidor at all times when not in use. An inhalation exposure system (Supplementary Figure 1) was designed and constructed to generate and deliver TS to a whole-body rat inhalation exposure chamber. The system automatically controlled and monitored chamber pressure, air flow, smoke concentration, $CO_2$, CO, temperature, relative humidity, and exposure time using custom software.

Tobacco smoke was generated using the inExpose Smoking Machine (SCIREQ Scientific Respiratory Equipment Inc, Montreal, Canada). The smoking machine used a 24-cigarette carousel. The cigarettes were lit and smoked by the machine in groups of 8. The machine drew a single puff from cigarette 1,

then move to cigarette 2, and so on until the eighth cigarette. The machine would then repeat this pattern 10 times resulting in 10 total puffs per cigarette. After 3 groups of 8 (24 total cigarettes), a new carousel was loaded as needed until the desired exposure dose was reached. A smoke puff was generated every 7.5 s while a bank of 8 cigarettes were active. The puff flow profile was set to a standard human smoking profile (International Standard ISO 3308). For reference, this flow is a bell-shaped curve with a duration of 2.0 s, a total volume of 35 ml, and a puff frequency of 1 every 60 s per cigarette.

The mainstream smoke puffs generated by the smoking machine were mixed with a constant stream of filtered air (45 l/min) provided by a mass flow controller (MCRW-50, Alicat Scientific, Tucson, Arizona). This provided enough ventilation for the exposure chamber to maintain $CO_2$ at levels $\leq$ 5000 ppm which were continuously monitored using an electronic probe (GMP222 0–10 000 PPM, Vaisala Corporation, Helsinki, Finland) placed in the exposure chamber's exhaust air stream. CO levels were also continuously monitored and maintained below 190 ppm by the software using a CO monitor (5001-B, NOVA Analytical Systems, Niagara Falls, New York) and a mass flow controller (MC-5-DS, Alicat Scientific) with its downstream port connected to house vacuum to remove portion of the smoke and $CO_2$ before it was mixed with the dilution air.

An airtight 22 $\times$ 22 $\times$ 40 in. ($L \times W \times H$) exposure chamber was constructed out of 16-gauge stainless steel with a clear polycarbonate door. Two stainless steel cage racks that could hold up to 12 rats each in individual cage partitions were used to house animals during exposures. The cage rack rested on top of cage support beams which were stainless steel tubes (3/8 in. outside diameter) with small holes (0.13-in. diameter) drilled into the undersides. The holes were placed at the center of each cage partition such that smoke would be drawn to each animal's breathing space. The exposure chamber air was exhausted into a carbon/HEPA filter bank. The exhaust air flow was controlled by a mass flow controller (MCRW-50-DS, Alicat Scientific) that had its downstream port connected to house vacuum. During exposures, this flow was automatically controlled by the exposure system software to maintain the pressure inside the exposure chamber at zero. Exposure chamber pressure was monitored using a differential pressure transducer (Model 264, Setra Systems, Inc, Boxborough, Massachusetts). The temperature and relative humidity inside the exposure chamber were also continuously monitored using an electronic probe (HMP60, Vaisala Corporation) and maintained at 73.4 $\pm$ 1.3°F and 36.7 $\pm$ 5.6%, respectively, throughout the exposure.

The TS aerosol mass concentration inside the exposure chamber was continuously monitored with a Data RAM (DR-40000) (Thermo Andersen Co, Smyrna, Georgia) and gravimetric determinations (37 mm cassettes with 0.45 μm pore-size Teflon filters, 0.2 l/min sample flow) were used to calibrate and verify the Data RAM readings during each exposure run. For this study, a 3-h average concentration of 80 mg/m$^3$ was the daily target. Aerosol particle size data were collected using a 10-stage impactor (MOUDI model 110-R, TSI Inc, Shoreview, Minnesota) with greased foils on each stage.

*Exposure of rats to silica and tobacco smoke aerosols*. The 24 rats used in this study, following their acclimatization to the animal facility conditions, were divided into 2 equal groups. The group 1 rats were exposed by whole-body inhalation to the TS aerosol, whereas the group 2 rats were simultaneously exposed to filtered air. The TS total particulate matter concentration in the exposure chamber was maintained at target level of 40 and 80 mg/m$^3$, respectively, during the first and second week of exposure. The target level of TS was set at 80 mg/m$^3$ in order to limit the concentration of CO generated in the chamber to $<$ 200 ppm. Furthermore, the target level of TS during the first week of exposure was maintained at a lower concentration of 40 mg/m$^3$ for acclimatization of the rats to TS exposure. The whole-body inhalation exposure to TS aerosol was done for 3 h/day on 2 nonconsecutive days/week. During the third week of the study, one half of the rats each from groups 1 and 2 were exposed by whole-body inhalation to the CS aerosol at a target concentration of 15 mg/m$^3$, 6 h/day for 5 consecutive days. The CS exposure conditions were selected based on the results of our previous studies (Sellamuthu *et al.*, 2011, 2013). The remaining rats belonging to both the groups were simultaneously exposed to air. No rats were exposed to TS during week 3. From the fourth week onwards, the rats were exposed to air or TS for a period of 6 months exactly as was done during the second week of the study resulting in 4 groups of rats—exposed to air, TS, CS, or CS plus TS. At the end of the 6 months exposure period, the rats were euthanized to determine pulmonary toxicity as described in the following sections.

*Euthanasia of rats and collection of biospecimens*. The rats were euthanized with an intraperitoneal injection of $\geq$ 100 mg sodium pentobarbital/kg body weight (Vortech Pharmaceuticals, Dearborn, Michigan). Blood collected directly from the abdominal aorta was transferred to Vacutainer tubes (Becton-Dickinson, Franklin Lakes, New Jersey) containing EDTA as an anticoagulant and mixed well by rotating the tubes. The right lung of the rats was clamped off and bronchoalveolar lavage (BAL) was performed in the left lung as previously described (Roberts *et al.*, 2014). The cellular and acellular fractions of the BAL were separated by centrifuging the samples (570 $\times$ g, 15 min, 4°C). The cell pellet obtained was resuspended in 1 ml PBS buffer and used for determination of pulmonary toxicity as described in the corresponding sections below. The diaphragmatic and cardiac lobes of the unlavaged right lung were inflated with 10% neutral buffered formaldehyde and stored in the same solution for histopathological analysis. The apical lobe of the unlavaged right lung was cut into pieces, weighing approximately 30 mg each, and stored in RNALater (Invitrogen, Carlsbad, California) and used to determine gene expression profile.

*Hematology*. Various hematological parameters, listed in Table 1, were determined in unclotted blood samples using an IDEXX Procyte instrument (IDEXX Corporation, Westbrook, Maine) following the procedures described in the user guide.

*Lung histology*. The lung lobes fixed in formaldehyde were paraffin embedded, sectioned at a thickness of 5 μm, stained with hematoxylin and eosin or Masson's trichrome stain and examined by a pathologist (Temple Health, Philadelphia, Pennsylvania). The lung histopathological changes were scored as none (normal histology), minimal ($<$ 10% thickening of alveolar walls in focal areas with little or no inflammatory cells occupying $<$ 10% of the lung parenchyma and 1 or 2 small foci per section), mild (10%–25% thickening of alveolar walls in focal areas with few inflammatory cells occupying 10%–20% of lung parenchyma and 1 or 2 large foci/section), or moderate (approximately 2-fold thickening of the alveolar walls in focal areas with plenty of inflammatory cells occupying 20%–40% of the lung parenchyma and 2–5 large foci/section).

**Table 1.** Hematology Parameters in Rats Exposed to Air, Tobacco Smoke, Silica, or Silica Plus Tobacco Smoke

| Parameter | Air | Tobacco Smoke | Silica | Silica + Tobacco Smoke |
|---|---|---|---|---|
| Red blood cells (RBC) (M/μl) | $8.89 \pm 0.08^{b}$ | $9.06 \pm 0.08^{a,b}$ | $8.92 \pm 0.04^{b}$ | $9.19 \pm 0.10^{a}$ |
| Hemoglobin (HGB) (g/dl) | $14.50 \pm 0.05^{b}$ | $14.63 \pm 0.11^{a,b}$ | $14.38 \pm 0.09^{b}$ | $14.85 \pm 0.18^{a}$ |
| Hematocrit (HCT) (%) | $43.85 \pm 0.31^{b}$ | $44.82 \pm 0.34^{a,b}$ | $44.07 \pm 0.26^{b}$ | $45.65 \pm 0.60^{a}$ |
| Mean corpuscular hemoglobin concentration (MCHC) (g/dl) | $33.07 \pm 0.26^{a}$ | $32.65 \pm 0.10^{a,b}$ | $32.63 \pm 0.11^{a,b}$ | $32.52 \pm 0.10^{b}$ |
| Reticulocytes (RET) (K/μl) | $285.40 \pm 5.30^{a}$ | $244.87 \pm 6.74^{b}$ | $281.67 \pm 9.21^{a}$ | $253.83 \pm 7.14^{b}$ |
| Reticulocytes (RET) (%) | $3.21 \pm 0.05^{a}$ | $2.70 \pm 0.05^{b}$ | $3.16 \pm 0.10^{a}$ | $2.77 \pm 0.10^{b}$ |
| White blood cells (WBCs) (K/μl) | $3.76 \pm 0.12^{b}$ | $4.51 \pm 0.18^{a}$ | $4.30 \pm 0.35^{a,b}$ | $4.73 \pm 0.27^{a}$ |
| Neutrophils (K/μl) | $0.87 \pm 0.08^{c}$ | $1.19 \pm 0.05^{b}$ | $1.40 \pm 0.07^{a}$ | $1.40 \pm 0.05^{a}$ |
| Neutrophils (%) | $22.98 \pm 1.57^{c}$ | $26.67 \pm 0.83^{b}$ | $32.92 \pm 1.37^{a}$ | $29.77 \pm 0.58^{a,b}$ |
| Lymphocytes (%) | $71.65 \pm 1.75^{a}$ | $68.78 \pm 0.54^{a}$ | $61.53 \pm 1.05^{c}$ | $65.10 \pm 0.71^{b}$ |

Only those parameters that showed a statistically significant ($p < .05$) difference in at least one of the exposure groups, compared with the controls (Air), are presented. A difference in the alphabet(s) in superscript following the SE indicates statistical significance ($p < .05$) among the 4 groups of rats.

*Lactate dehydrogenase activity*. Lactate dehydrogenase (LDH) activity in the acellular BAL fluid (BALF) was determined with a COBAS C111 analyzer (Roche Diagnostic Systems, Mount Clair, New Jersey) as previously described (Sellamuthu et al., 2011).

*BAL cell counts*. The cellular fraction of BAL was resuspended in 1 ml of PBS buffer and the total number of BAL cells was determined using a Coulter Multisizer II and Accu Comp software (Coulter Electronics, Hialeah, Florida). BAL cells ($5 \times 10^4$) were spun onto microscope slides using a Cytospin 3 centrifuge (Shandon Life Sciences International, Cheshire, England) and stained with a Leukostat stain (Fisher Scientific, Pittsburgh, Pennsylvania) to differentiate alveolar macrophages (AMs) and polymorphonuclear leukocytes (PMN). In total, 200 cells were counted per rat and percentages were multiplied back across the total cell count to obtain total number of AM and PMN.

*BALF cytokines, chemokines, and growth factors*. The BALF levels of 27 rat cytokines, chemokines, and growth factors were determined using a MILLIPLEX Rat Cytokine/Chemokine 27-plex kit (Millipore, St Charles, Missouri) and a Luminex 100 system (Luminex, Austin, Texas) by Eve Technologies Corporation (Calgary, Alberta, Canada). The 27-plex consisted of G-CSF, Eotaxin, GM-CSF, IL-1α, Leptin, MIP-1α, IL-4, IL-1β, IL-2, IL-6, EGF, IL-13, IL-10, IL-12 (p70), IFNγ, IL-5, IL-17, IL-18, MCP-1, IP-10, GRO/KC, VEGF, Fractalkine, LIX, MIP-2, TNF-α, and RANTES.

*Reactive oxygen species generation by BAL cells*. A previously described luminol-dependent chemiluminescence (CL) assay (Roberts *et al.*, 2014) was performed to determine the generation of reactive oxygen species (ROS) by the lung phagocytes (AM and PMN). Phorbol 12-myristate 13-acetate (PMA), stimulant of AM and PMN, and nonopsonized, insoluble zymosan, a stimulant of AM only, were used to determine the contribution of both AM and PMN to the overall production of ROS in the rat lungs. A BAL cell volume equivalent to $5 \times 10^5$ total BAL cells or $5 \times 10^5$AM was incubated with luminol for 10 min at 37°C prior to stimulating the cells with either 10 M PMA or 2 mg/ml zymosan, respectively. Baseline oxidant production by the BAL cells was measured in the absence of the stimulants. Measurement of CL was recorded using a Berthold LB 953 luminometer (Wildbad, Germany) for 15 min at 37°C, and the integral of counts per minute (cpm) per 1 million cells versus time was calculated. Chemiluminescence was calculated as the cpm of the stimulated cells minus the cpm of the corresponding resting cells, and the value was normalized to the total number of BAL cells for PMA-stimulated CL and total number of AM for zymosan-stimulated CL.

*Lung gene expression profile*. A piece of the lung tissue stored in RNALater was used to isolate total RNA free of contaminating DNA and proteins using miRNEasy Mini Kit (Qiagen, Inc, Valencia, California) following the procedure, including the on-column DNase digestion, provided by the manufacturer. The integrity and purity of the RNA samples isolated were determined using an Agilent 2100 Bioanalyzer and RNA 6000 Nano Kit (Agilent Technologies, Palo Alto, California). Total RNA was quantified by UV-Vis spectrophotometry. Only RNA samples exhibiting an RNA integrity number $\geq 8.0$ were used in the gene expression studies.

One microgram total RNA/sample was used to create sequencing libraries using the Illumina TruSeq Stranded Total RNA Library Prep Kit (Illumina, Inc, San Diego, California) following the protocol provided by the manufacturer. Stated briefly, following depletion of ribosomal RNA, the RNA samples were purified and fragmented (68°C for 5 min). The RNA fragments were purified using a bead cleanup procedure and reverse transcribed into first strand cDNA using reverse transcriptase and random primers. While synthesizing the double-stranded cDNA, deoxyuridinetriphosphate (dUTP) was incorporated in place of deoxythymidine triphosphate (dTTP) followed by the addition of a single "A" nucleotide to the 3′ ends to facilitate proper adapter ligation. Indexing adapters provided in the library preparation kit were ligated to the ends of the ds cDNA. After adapter ligation, the samples were PCR amplified (12 cycles) to enrich the DNA fragments containing the adapter molecules and to enhance the amount of DNA in the library using a Veriti 96 Well Thermal Cycler (Applied Biosystems, Foster City, California). The PCR amplified cDNA library samples were quantified using a dsDNA HS Assay Kit (Invitrogen by ThermoFisher Scientific, Waltham, Massachusetts) and Qubit 3.0 Fluorometer (Invitrogen by ThermoFisher Scientific). Average fragment size and fragment distribution of the cDNA library samples were then assessed using an Agilent 2100 Bioanalyzer with High Sensitivity DNA Reagents (Agilent Technologies, Santa Clara, California).

Individual sample libraries were provided to the Centers for Disease Control and Prevention Genome Sequencing Laboratory (GSL; Atlanta, Georgia) for $2 \times 100$ base pair, paired-end sequencing using the Illumina Hiseq 2500 (Illumina, San Diego, California) in rapid run mode using HiSeq Rapid Cluster Kit v2 (Illumina) and HiSeq Rapid SBS Kit v2 (Illumina). After the

library sequences were demultiplexed by the GSL, the quality of each sample library was assessed with respect to the number of reads per sample, mean quality score, and FASTQC parameters (Andrews, 2010). Reads were then processed using Trimmomatic/0.35 with the options PE, ILLUMINACLIP:TruSeq2-PE.fa:2:30:10 LEADING:3 TRAILING:3 SLIDINGWINDOW:4:15 MINLEN:85 to remove any remaining adapter sequence, low quality reads, low quality read ends, and sequences shorter than 85 bases in length (Bolger *et al.*, 2014). Sequence quality was then reevaluated via FASTQC. All sequences that passed the trimming and quality control with both reads in a pair present were aligned to the *Rattus norvegicus* Rnor 6.0 genome from NCBI downloaded July 31, 2015 using HiSat2/2.1.0 (Kim *et al.*, 2015). Raw gene counts were assigned using Samtools/1.9 (Li et al., 2009), Python/2.7.3 and HTSeq/0.6.1. Rnr1 (Ribosomal 45S Cluster 1) and Rnr2 (Ribosomal 45S Cluster 2) displayed extremely high counts and were manually removed before further analysis. Using edgeR, raw counts were converted to counts per million (CPM), log-CPM, and normalized using the trimmed mean of *M*-values method. Finally, differentially expressed genes were calculated using limma (Law *et al.*, 2016; R Core Team, 2018). Significantly differentially expressed genes (SDEGs) were those genes with an absolute fold change $> 1.5$-fold and an adjusted $p$ value $< .05$.

*Quantitative real-time polymerase chain reaction analysis*. Nine of the SDEGs identified by NGS analysis in the CS only exposed lung samples, compared with the control samples, were selected for quantitative real-time polymerase chain reaction (QRT-PCR) analysis to confirm differential expression. The nucleotide sequences of the primers used in the QRT-PCR analysis of the target genes and the house-keeping gene (β-actin) can be found in our previous publication (Sellamuthu *et al.*, 2013). Reverse transcription of RNA to synthesize cDNA was conducted using the Advantage RT-for-PCR-Kit (Takara Bio USA, Mountain View, California). The QRT-PCR amplification, detection of the amplified PCR products, and their quantitation were conducted with a 7900 HT Fast Real Time PCR machine and SYBR Green PCR MasterMix (Applied Biosystems). The expression levels of the target genes were normalized using that of β-actin, the house-keeping gene.

*Bioinformatic analysis of gene expression data*. Bioinformatic analysis of the SDEGs was conducted using Ingenuity Pathway Analysis (IPA) software (Qiagen, Inc, Valencia, California). The IPA program is designed to map the biological relationship of the input genes and classify them into categories of biological functions, canonical pathways, diseases, and networks.

*Statistical analysis of data*. All data with the exception of NGS data between the exposed and control groups were compared using the one-way analyses of variance. Post hoc comparisons were made with Fisher's least significant difference test. Analyses were performed using JMP version 13.2 for Windows. The level of statistical significance was set at $p < .05$.

## RESULTS

### *Test Atmospheres*

The mass median aerodynamic diameter of CS and TS particles present in the aerosols generated for rat inhalation exposure was 1.69 μm ($\sigma_g = 1.9$) and 0.469 μm ($\sigma_g = 1.75$), respectively (Supplementary Figs. 2 and 3). Based on the mass weight filter measurements, the actual aerosol concentrations of CS and TS particulate matter in the rat exposure chamber were $16.25 \pm 2.3$ and $78.7 \pm 5$ mg/m$^3$, respectively. The alveolar lung burden of CS and TS resulting from inhalation exposure of rats under the study conditions estimated using the MPPD model (Anjilvel and Asgharian, 1995) was 51 and 7974 μg, respectively. The rat exposure to CS employed in our study corresponded to a worker being exposed to CS for 40 years at 1.2 μg/m$^3$ (Gehr *et al.*, 1978; National Institute for Occupational Safety and Health, 1976; Ohashi *et al.*, 1994). Similarly, the TS exposure employed in the rats corresponded to a human smoking 2.33 cigarettes/day for 6 months (Chen *et al.*, 1990).

### *Clinical Effects*

The terminal body weights of the rats exposed to TS alone or TS plus CS were approximately 3% less compared with those exposed to air or CS alone (data not presented). Except for the slight body weight loss noticed among the TS- and TS plus CS-exposed rats, no other clinical sign of toxicity was detected in any of the rats.

### *Lung Gross Morphology and Histology*

The gross lung morphology of the TS alone-exposed rats was normal and same as that of the control, air-exposed rats (Supplementary Figure 4). On the other hand, inhalation exposure of rats to CS resulted in a mild nodular appearance of the lungs consisting of few, off-white patches. A quantitative increase with respect to the nodular appearance of the lungs was observed among the rats exposed to both TS and CS, compared with exposure to CS alone (Supplementary Figure 4).

The lungs of all control, air-exposed rats exhibited normal histology (Figure 1A). The only histological change noticed in the lungs of the TS alone-exposed rats was a slight increase in the number of AM and PMN infiltrated into the lungs (Figure 1B). Inhalation exposure of rats to CS alone resulted in mild changes in lung histology. The main lesion detected in the lungs of the CS-exposed rats was focal cellular alveolitis (FCA) which consisted of an approximately 2-fold thicker alveolar wall, compared with the normal, in association with accumulation of AMs, PMNs, fibroblasts, and AP2 cells (Figure 1C). Most of the CS-exposed lungs showed up to 2 FCAs per lung section. The increased thickness of the alveolar wall was further confirmed with trichrome stain (Supplementary Figure 5). The histological changes detected in the CS plus TS-exposed rat lungs were similar to those exposed to CS alone except for slight quantitative increases in the lesions. The alveolar wall was 2–3-fold thicker compared with normal and the number of FCAs per lung section was 3–5. In addition, 2 out of 6 CS plus TS-exposed rat lungs showed the presence of small granuloma (Supplementary Figure 6) that was not detected in the rats exposed to CS alone.

### *BAL LDH and Cell Counts*

BALF LDH activity, an indicator of lung cytotoxicity, did not change in the lungs of the TS alone-exposed rats compared with the control, air-exposed rats (Figure 2A). CS exposure, both alone and with TS, resulted in a statistically significant increase ($p < .05$) in BALF LDH activity compared with both the control (air) and TS alone-exposed rats (Figure 2A). Similar to the BALF LDH activity, the number of BAL cells (total, AMs, and PMNs) detected in the lungs of the rats exposed to TS alone was comparable to that of the air-exposed controls (Figs. 2B–D). On the other hand, statistically significant increases in the number of the total BAL cells, AMs, and PMNs were detected in the rat

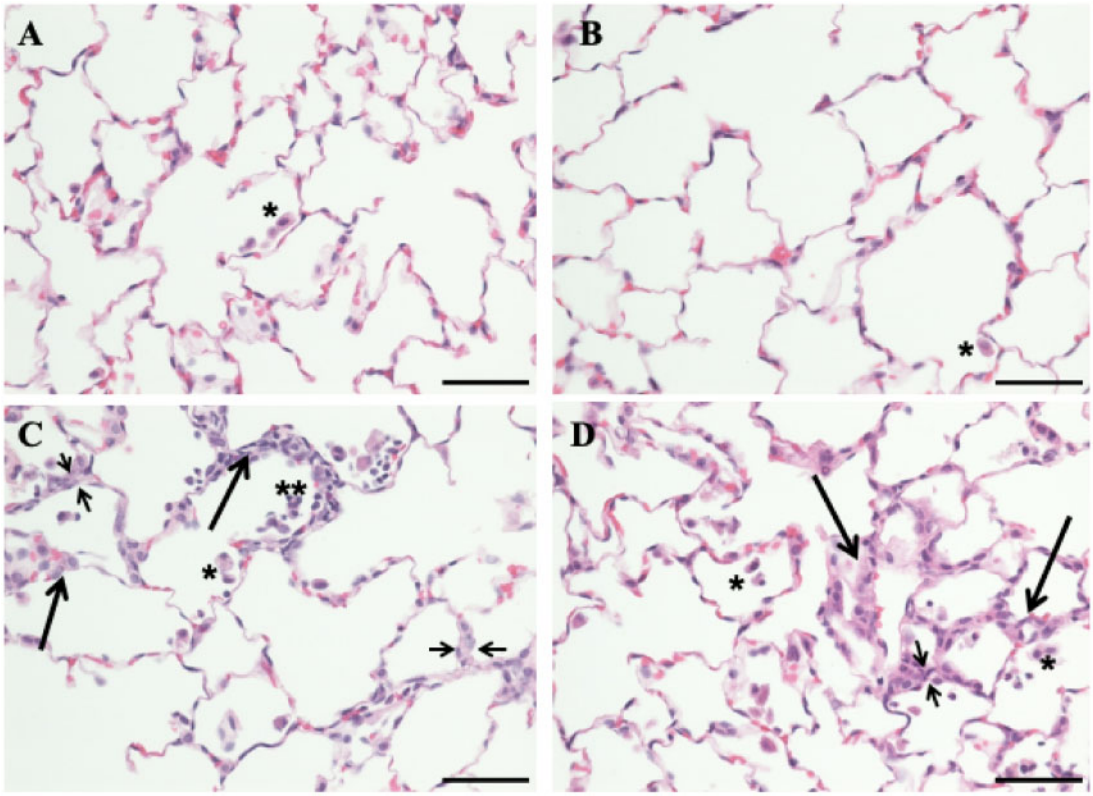


**Figure 1.** Photomicrographs of lung sections from the control, tobacco smoke (TS)-, crystalline silica (CS)-, and TS plus CS-exposed rats. Rats were exposed to air, CS, TS, or TS plus CS as described in the text. Lung sections were stained with hematoxylin and eosin. Normal pulmonary architecture with occasional intra-luminal alveolar macrophages (single asterisk) was noted in air alone-exposed (A) and TS alone-exposed animals (B). Rats exposed to CS alone (C) and those exposed to TS plus CS (D) showed increased intra-alveolar macrophages (single asterisk) as well as occasional polymorphonuclear leukocytes inside the alveolar lumina (double asterisks). Areas of focal interstitial alveolitis (long thicker arrows) were seen in both the CS- and CS plus TS-exposed groups (C and D). These lesions consisted of thickened alveolar walls (indicated by short thinner arrows) with increased number of macrophages, pneumocytes, and round mononuclear cells. The bar in all panels equals 50 μm and the magnification ×400.

lungs exposed to CS alone or CS plus TS. The increase in cell number was most significant in the case of PMNs which was 141- and 490-fold higher in the CS- and CS plus TS-exposed rat lungs, respectively, compared with those exposed to air alone (Figure 2D). In addition, all BAL parameters of lung toxicity (LDH activity, number of total cells, AMs, and PMNs) exhibited a statistically significant difference ($p < .05$) between the CS alone- and CS plus TS-exposed rat lungs.

### *Oxidant Generation by BAL Phagocytes*

The generation of reactive oxidants by the BAL phagocytes obtained from the TS alone-exposed rats, in the presence of zymosan or PMA, was comparable to that generated by the air-exposed, control phagocytes (Figure 3). On the other hand, the zymosan and PMA-stimulated oxidant generation by the phagocytes obtained from the CS alone-exposed rats showed a 17- and 77-fold increase, respectively, compared with the controls. A further and statistically significant increase in both the zymosan- and PMA-stimulated oxidant generation (30- and 188-fold increase, respectively) compared with the controls was detected in the phagocytes obtained from rats exposed to CS plus TS.

### *Hematology*

Many of the hematological parameters measured were significantly affected by exposure of the rats to TS, CS, and/or CS plus TS (Table 1). However, the number of hematological parameters that were significantly affected was more in the group that was exposed to CS plus TS compared with those exposed to the agents individually. The number of white blood cells was higher in all 3 groups of the exposed rats, compared with the controls, and this was associated with a corresponding increase in the percent of neutrophils present in the blood. Conversely, the percent of lymphocytes decreased in all 3 groups of the exposed rats compared with the air controls.

### *BALF Cytokines*

The BALF levels of several of the cytokines analyzed were significantly affected by exposure of the rats to TS, CS, or CS plus TS (Figure 4 and Supplementary Table 1). Compared with the air controls, the BALF levels of only 3 cytokines (G-CSF, IL-12, and IL-5) were significantly different in the TS only exposed rats. On the other hand, exposure of rats to CS alone resulted in significant differences in the BALF levels of 11 cytokines (GM-CSF, IL-1α, MIP-1α, IL-18, MCP-1, IP-10, VEGF, LIX, MIP-2, TNF-α, and RANTES) compared with the air controls. The most significant change was noticed in the case of LIX which showed a 19-fold increase in the CS-exposed rats compared with the controls. Exposure to CS plus TS, compared with air, resulted in significant changes in the BALF levels of 2 more cytokines (EGF and GRO/KC) in addition to the 11 cytokines which were significantly affected by the CS alone exposure.

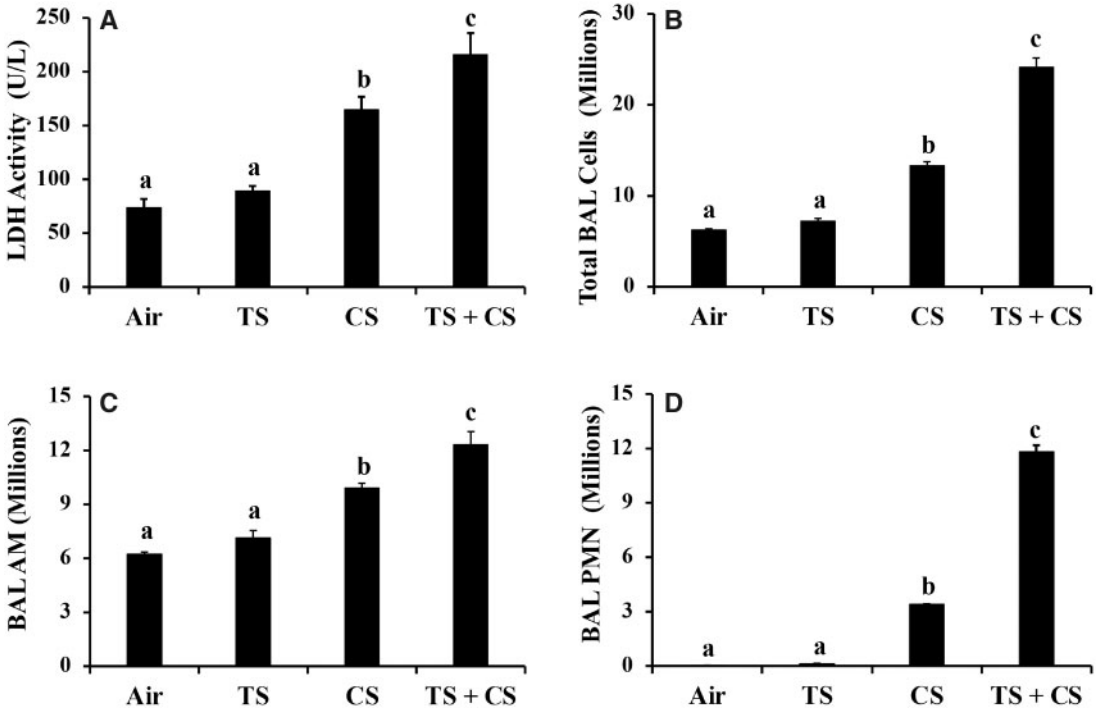


**Figure 2.** Bronchoalveolar lavage parameters of lung response in the air, tobacco smoke (TS)-, crystalline silica (CS)-, and TS plus CS-exposed rats. Groups of rats were exposed to air, CS, TS, or TS plus CS and lung lavage was performed following euthanasia as described in the text. Bronchoalveolar lavage (BAL) parameters of lung response, viz, lactate dehydrogenase (LDH) activity (A), total BAL cells (B), alveolar macrophages (AMs) (C), and PMNs (D) were determined as described in the text. Data represent mean ± SE ($n = 6$). Statistical significance ($p < .05$) among the different groups of rats is represented by differences in the letters (a, b, and c) above the corresponding bars.

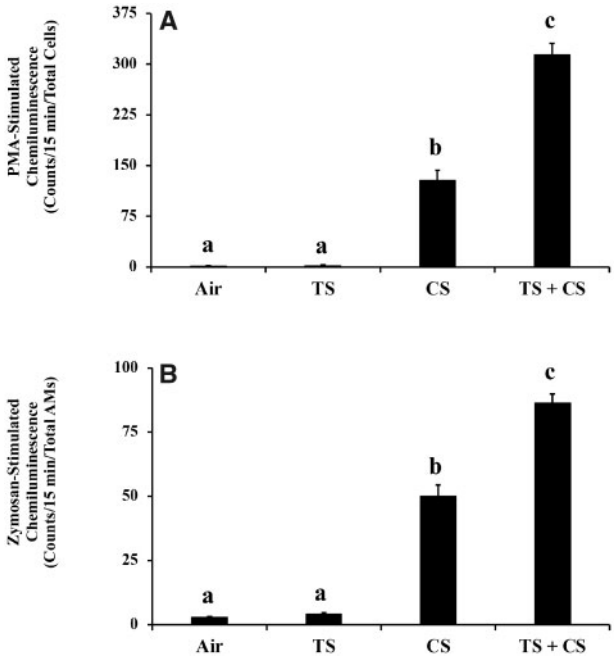


**Figure 3.** Oxidant generation by bronchoalveolar lavage (BAL) phagocytes in the air, tobacco smoke (TS)-, crystalline silica (CS)-, and TS plus CS-exposed rats. Groups of rats were exposed to air, TS, CS, or TS plus CS and the generation of oxidants by the BAL cells isolated following euthanasia and lung lavage were determined as described in the text. A, Oxidant generation by AMs and PMN. B, Oxidant generation by AMs. Data represent mean ± SE ($n = 6$). Statistical significance ($p < .05$) among the different groups of rats is represented by differences in the letters (a, b, and c) above the corresponding bars.

*Lung Gene Expression Profile*

NGS analysis detected 16 588 transcripts in the lungs of the rats (Supplementary Table 2). Among the transcripts detected, compared with the air controls, the expressions of 16, 610, and 1571 transcripts were significantly different (fold change > 1.5 and FDR $p < .05$) in the TS-, CS-, or CS plus TS-exposed rat lungs, respectively (Figure 5A). In each of the exposed groups, the number of overexpressed transcripts was much higher compared with the downregulated genes. In general, the number of SDEGs (total, upregulated, and downregulated) detected in the rat lungs corresponded to the severity of the pulmonary toxicity induced by the agent(s). Six of the SDEGs detected were common in all 3 exposure groups, whereas 3, 103, and 1057 SDEGs were unique to the TS, CS, or CS plus TS exposure group, respectively (Figure 5B). The fold changes in expressions of many of the SDEGs also corresponded of the severity of lung toxicity being highest in the CS plus TS group which was followed by the CS and the TS group, respectively (Table 2). Results of the RT-PCR analysis confirmed the findings of NGS analysis (Table 3).

*Bioinformatic Analysis of the SDEGs*

The number of biological functions and diseases, canonical pathways, and networks significantly enriched in the rat lungs corresponded to the alterations in the various lung toxicity parameters detected in the rats. A highest number of significantly enriched IPA biological functions and diseases, canonical pathways, and networks were detected in the lungs of the CS plus TS-exposed group of the rats which also exhibited the most significant changes in the various parameters assessed to determine lung toxicity in response to their exposure to the

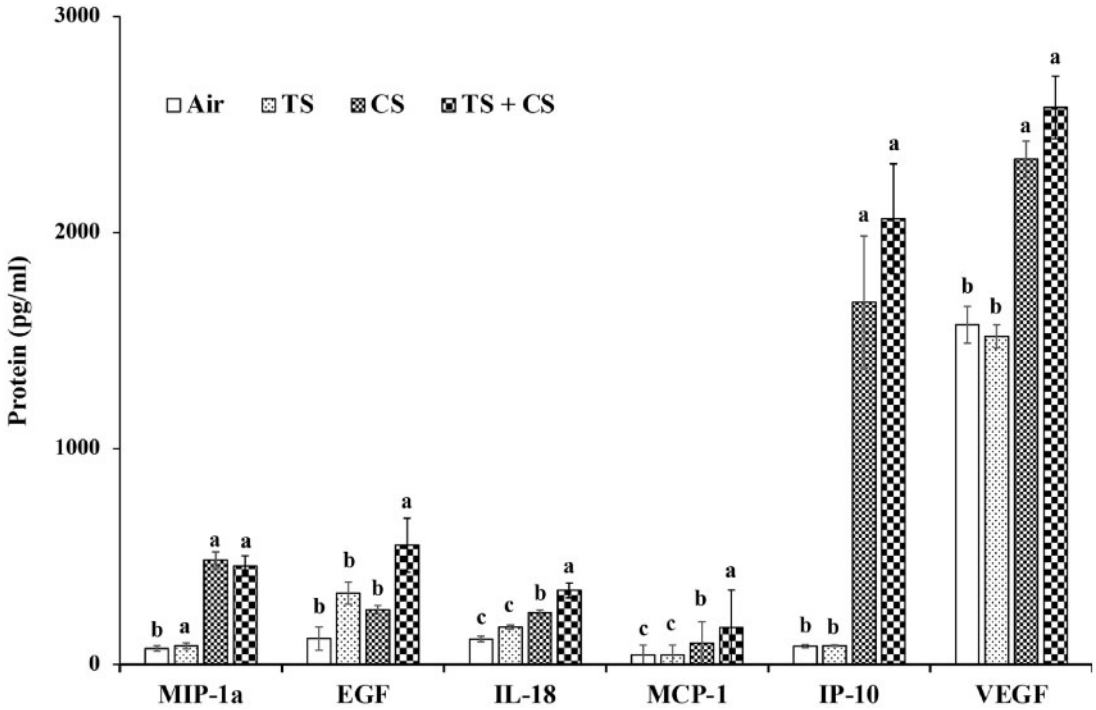


**Figure 4.** Cytokines in the bronchoalveolar lavage fluid (BALF) of the air, tobacco smoke (TS)-, crystalline silica (CS)-, and TS plus CS-exposed rats. Groups of rats were exposed to air (control), TS, CS or TS plus CS and the BALF obtained following euthanasia of the rats and lung lavage were analyzed for various cytokines and chemokines as described in the text. Data represent mean ± SE ($n = 6$). Statistical significance ($p < .05$) among the different groups of rats is represented by the differences in the letters (a, b, and c) above the corresponding bars. BALF levels of the remaining cytokines analyzed in the rats are presented in Supplementary Table 1.

toxic agent(s). Some of the top-ranking IPA biological functions and diseases that were significantly enriched in the lungs of the rats exposed to CS were respiratory diseases, cellular growth and proliferation, free radical scavenging, cell death and survival, cell-to-cell signaling and interaction, inflammatory diseases, inflammatory response, organismal injury and abnormalities, cancer, immune cell trafficking, and cellular movement (Figure 6). It is noteworthy that the enrichment of all these disease and biological function categories, as represented by the number of SDEGs belonging to each of them, was highest among the CS plus TS group followed by the CS and the TS group, respectively. For example, the number of SDEGs that belonged to the IPA category, cancer, was 6, 274, and 642, respectively, in the TS, CS, and CS plus TS group of rats. Similar observations were made with respect to the significantly enriched canonical pathways or networks and the various lung toxicity parameters assessed in the rats (Supplementary Tables 3–5). These results, therefore, demonstrated an overall agreement between the results obtained from the bioinformatic analysis of the SDEGs and the severity of lung toxicity detected in the rats exposed to the toxic agent(s).

Bioinformatic analysis of the SDEGs further supported the very low pulmonary response noticed in the rats exposed to TS alone as well as exacerbation of the CS-induced pulmonary response by the TS exposure. This is illustrated, for example, by the results of the significantly enriched cancer-related IPA biological functions detected in the 3 groups of the rats (Figure 7). No cancer-related biological function was significantly ($p < .05$) enriched in the lungs of the rats exposed to TS alone. Exposure of the rats to CS alone resulted in a significant enrichment of 102 cancer-related functions in their lungs. On the other hand, the combined exposure of rats to CS and TS resulted in a significant enrichment of 156 cancer-related functions including 62 unique functions.

## DISCUSSION

Human exposure to TS may result in significant morbidity and mortality (U.S. Department of Health and Human Services [USDHHS], 2014) because it contains many chemicals, particles, and gases including well characterized mutagens and carcinogens (Roemer *et al.*, 2012; Schaller *et al.*, 2016). It is estimated that millions of Americans are living with a TS exposure-related disease resulting in hundreds of billions of dollars in health care cost alone (Xu *et al.*, 2015). Although smoking is the number one cause for lung cancer, other pulmonary outcomes of exposure to TS include asthma, COPD, emphysema, and chronic bronchitis (USDHHS, 2014). Despite the significant decline in the prevalence of adult cigarette smoking, TS exposure remains the number one preventable cause of diseases and death in the United States (USDHHS, 2014).

The pulmonary toxicity in response to exposure of rats to TS has been investigated previously (Carter and Misra, 2010; Choi *et al.*, 2016; Dorman *et al.*, 2012) by employing the reference cigarette (3R4F) that was used in the present study. Compared with the previous studies, which reported significant loss in body weight and induction of lung toxicity in the TS-exposed rats, no adverse effects except a marginal (< 3%) loss in body weight and mild lung inflammation were detected in our rat model. Our results, therefore, suggested that the TS exposure conditions employed in our study were below the threshold required to result in any significant toxicity in the rats.

Human exposure to dust is almost unavoidable and silica, the most abundant mineral present in the earth's crust, can be a major constituent of dust. Exposure to CS, like TS, especially

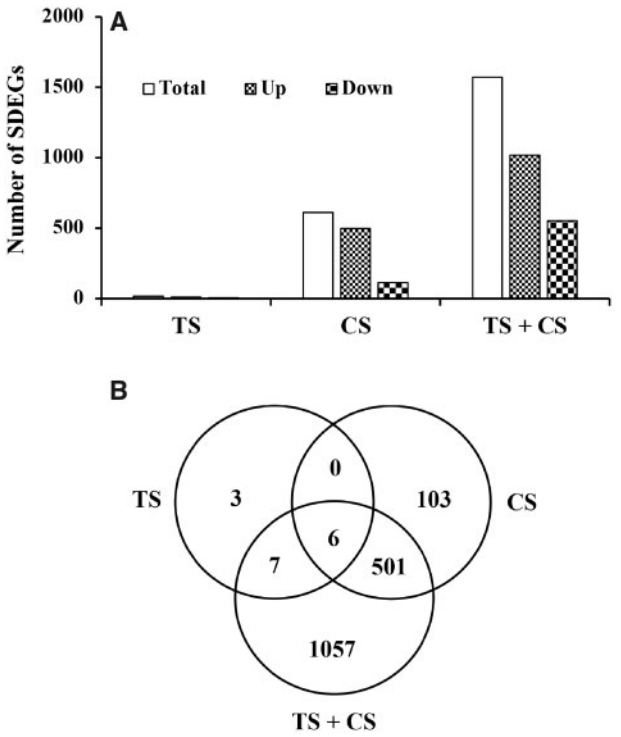


**Figure 5.** Differentially expressed genes in the lungs of the of the tobacco smoke (TS)-, crystalline silica (CS)-, and TS plus CS-exposed rats. Global gene expression profiles in the rat lungs were determined by next generation sequence analysis as described in the text. Significantly differentially expressed genes (SDEGs) are those with a fold change $> 1.5$ and an adjusted $p$ value $< .05$ compared with the control (air) group. A, The number of total, upregulated, and downregulated SDEGs in each exposure group of the rats compared with the control group. B, Venn diagram of the SDEGs showing the number of unique and overlapping genes in each exposure group.

at levels exceeding the OSHA PEL, is known to have a significant impact on human respiratory health. CS is a human carcinogen (IARC, 1997) and can cause silicosis (Greenberg *et al.*, 2007), a progressive and potentially fatal fibrotic lung disease.

Crystalline silica particles are engulfed by AM for elimination from the lungs. The interaction of CS particles with the AM may result in AM damage and activation. The damaged/activated AMs release various molecules that act as mediators, playing key roles in the lung's response to CS exposure. The mediators released in response to the interaction of CS particles with the AM include ROS, reactive nitrogen species, free radicals, transcription factors, inflammatory cytokines and chemokines, growth factors, and fibrogenic factors (Greenberg *et al.*, 2007). The net result of the complex interactions between these molecules and lungs often causes lung damage potentially resulting in diseases such as silicosis and cancer. However, the actual molecular mechanisms underlying the complex interactions taking place among these molecules as well as with the lung resulting in CS-induced adverse health effects require further understanding. Furthermore, the molecular mechanisms underlying the potential modification of CS-induced pulmonary toxicity by confounders, for example TS exposure, need to be determined for a better understanding of the health effects associated with CS exposure.

Consistent with the results of our previous studies (Sellamuthu *et al.*, 2011, 2013), exposure to CS resulted in significant lung toxicity in the rats. This was evidenced by the significant increases in the BAL parameters of toxicity such as the LDH activity and the AM and PMN counts (Figure 2) and histological changes which included FCA, thickening of the alveolar epithelium, and collagen deposition (Figure 1 and Supplementary Figure 5) in the CS-exposed rats. A significant increase in the reactive oxidants generated by the BAL cells (Figure 3) and alterations in the BAL levels of cytokines and chemokines (Figure 4 and Supplementary Table 1) in the lungs of the CS-exposed rats, compared with the controls, provided additional evidence supporting the induction of lung toxicity by CS in our rat model.

Alterations in the various lung toxicity parameters determined in the CS plus TS-exposed rats were of a greater magnitude compared with those detected in the rats exposed to TS or CS alone. For example, exposure of rats to TS or CS alone resulted in 4- and 141-fold increase, respectively, in the BAL PMN cells. Exposure to TS in addition to CS, on the other hand, resulted in a 490-fold increase in the BAL PMN count compared with the air-exposed controls. The number of areas affected by FCA, thickening of the alveolar wall, and intensity of trichrome staining was more in the TS plus CS-exposed rat lungs compared with those exposed to the agents individually (Figure 1 and Supplementary Figure 5). Exposure of rats to CS alone did not result in granuloma formation. On the other hand, exposure to TS in addition to CS resulted in the formation of small granulomas in the lungs (Supplementary Figure 6). Similar differences were noticed between the CS alone- and CS plus TS-exposed rats with respect to the oxidants generated by the BAL phagocytes and the BALF levels of several cytokines/chemokines analyzed. Collectively, these results show that TS exposure exacerbated the CS-induced lung toxicity in the rats, in agreement with the previous report by Dorman *et al.* (2012). Decreased mucociliary clearance in TS-exposed lungs is known to result in prolonged retention of particles (Cohen *et al.*, 1979). Similarly, particles may affect the barrier properties of lung epithelium facilitating enhanced uptake and toxicity of the particles (Bhalla, 1999). However, the focus of the current study was the molecular mechanisms potentially underlying the exacerbated lung toxicity in response to exposure to CS and TS.

Gene expression changes taking place in target organs in response to exposure to a toxic agent may be the manifestation of the toxicity resulting from the exposure. Alternatively, exposure to a toxic agent may result in gene expression changes with corresponding alterations in the functions mediated by the affected genes which may ultimately result in target organ toxicity. Therefore, gene expression profiling in target organs followed by diligent bioinformatic analysis of the differentially expressed genes may provide information critical to the molecular mechanisms underlying the toxicity. The number of the SDEGs detected in the lungs (Figure 5) corresponded to the severity in lung toxicity (Figs. 1 and 2). Similarly, the fold changes in expressions of the vast majority of the SDEGs corresponded to the severity of lung toxicity detected in the rats (Tables 2 and 4). For instance, SPP1—a gene involved in lung inflammatory and fibrotic responses of toxic particles (Dong and Ma, 2017)—was overexpressed by 2.85-, 36.69-, and 72.61-fold, respectively, in the TS-, CS-, and TS plus CS-exposed rats, compared with the air controls. The vast majority of the top-ranking IPA diseases and biological function categories, canonical pathways, and networks that were significantly enriched in the rat lungs were those known to be involved in lung toxicity. Furthermore, the enrichment of each of the biological functions and disease categories corresponded to the severity of lung toxicity induced by the toxic agent(s). Collectively, these results suggested that the gene expression changes detected in the lungs were related to

**Table 2.** Top 20 Differentially Expressed Transcripts in the Rat Lungs

| Transcript | Fold Change in Expression Versus Control | | |
|---|---|---|---|
| | TS | CS | TS + CS |
| *Lactoperoxidase (LPO)* | 9.79 | 217.22 | 354.13 |
| *Secreted phosphoprotein 1 (SPP1)* | 2.85 | 36.69 | 72.61 |
| *Resistin like alpha (RETNLA)* | 1.23 | 15.80 | 31.34 |
| *Solute carrier family 26 member 4 (SLC26A4)* | 4.09 | 24.15 | 30.58 |
| *Orosomucoid 1 (ORM1)* | 1.84 | 12.77 | 28.70 |
| *C-C motif chemokine ligand 2 (CCL2)* | 3.49 | 18.75 | 26.84 |
| *BPI fold containing family B, member 1 (BPIFB1)* | 2.31 | 15.74 | 26.08 |
| *Copine 5 (CPNE5)* | 1.79 | 11.25 | 23.91 |
| *C-C motif chemokine ligand 7 (CCL7)* | 2.89 | 13.74 | 22.77 |
| *Transmembrane protein 72 (TMEM72)* | 2.56 | 6.63 | 20.92 |
| *Matrix metallopeptidase 12 (MMP12)* | 2.42 | 14.21 | 18.82 |
| *Chitinase, acidic (CHIA)* | 2.21 | 7.64 | 14.52 |
| *Complement factor I (CF1)* | 1.96 | 7.65 | 13.13 |
| *CD177 antigen-like (LOC100909700)* | 2.57 | 5.80 | 12.76 |
| *Kininogen 1 (KNG1)* | 1.37 | 5.48 | 12.42 |
| *Uncharacterized LOC102552631(LOC102552631)* | 3.14 | 10.62 | 12.38 |
| *Transmembrane protein 45 b (TMEM45B)* | 1.98 | 10.81 | 11.99 |
| *C-X-C motif chemokine ligand 6 (CXCL6)* | 4.06 | 21.96 | 11.97 |
| *Sodium voltage-gated channel alpha subunit 10 (SCN10A)* | 1.79 | 7.48 | 11.84 |
| *Immune-responsive gene 1 (IRG1)* | 1.33 | 3.51 | 11.73 |

The transcripts listed are the top 20 differentially expressed (FC > 1.5 and FDR $p < .05$) in the TS + CS group of rats. The fold changes in expressions of the same transcripts in the TS and CS group of rats are also presented for comparison.

**Table 3.** RT-PCR Validation of NGS Results

| Transcripts | Fold Change in Expression | |
|---|---|---|
| | NGS | RT-PCR[a] |
| *C-C motif chemokine ligand 2 (CCL2)* | 18.75 | 13.20 (8.32–20.94) |
| *C-C motif chemokine ligand 3 (CCL3)* | 2.95 | 1.90 (1.28–2.84) |
| *C-X-C motif chemokine ligand 1 (CXCL1)* | 2.93 | 2.22 (1.44–3.40) |
| *Lipocalin 2 (LCN2)* | 2.90 | 5.98 (4.23–8.46) |
| *Matrix metallopeptidase 12 (MMP12)* | 14.21 | 9.48 (6.22–14.45) |
| *Metallothionein 1a (MT1A)* | 1.76 | 1.93 (1.36–2.75) |
| *Solute carrier family 13 member 2 (SLC13A2)* | 2.80 | 2.03 (1.36–3.05) |
| *Solute carrier family 26 member 4 (SLC26A4)* | 24.15 | 15.66 (9.40–26.10) |
| *Superoxide dismutase 2 (SOD2)* | 2.38 | 1.71 (1.14–2.56) |

The data presented are for the CS group of rats compared with the controls (Air).
[a]Fold change range with standard deviation factored in.

the toxicity induced by the toxic agent(s) reflecting the severity of toxicity.

The role of oxidative stress in the pathological effects associated with CS exposure is well established (Sato *et al.*, 2018). Superoxide anion ($O_2^{\cdot-}$), a highly reactive and, therefore, toxic ROS is generated in cells by the activities of genes that belong to the nicotinamide adenine dinucleotide phosphate, reduced (NADPH) oxidase (NOXO) family (Bedard and Krause, 2007). The transcripts for several members of the NOXO family of genes, viz, *NOXO1*, *NCF1*, *NCF2*, *NCF4*, *DUOX1*, and *DUOXA1*, involved in oxidative stress-mediated toxicity (Ameziane-El-Hassani *et al.*, 2015; Carnesecchi *et al.*, 2009; Jacob *et al.*, 2012; Sato *et al.*, 2008), were significantly overexpressed, especially in the CS- and CS plus TS-exposed rat lungs, compared with the controls (Table 4). The fold changes in the expression of these genes (Table 4), corresponded to the severity of TS-, CS- and CS plus TS-induced lung toxicity (Figs. 1 and 2), suggesting their involvement, through the generation of ROS, in the lung toxicity induced by CS as well as the exacerbation of CS-induced lung toxicity by TS in the rats.

Hydrogen peroxide ($H_2O_2$), the dismutation product of $O_2^{\cdot-}$ mediated by the SUPEROXIDE DISMUTASE (SOD) enzyme, is reactive and may exert toxicity if not detoxified by CATALASE (Antunes *et al.*, 2002). Significant overexpression of the *SOD2* transcript with no corresponding increase in the *Catalase* transcript was detected in the CS- and CS plus TS-exposed rat lungs (Table 4). Such a scenario is favorable for the accumulation of toxic $H_2O_2$ in the CS- and CS plus TS-exposed rat lungs and may contribute to the toxicity detected. LACTOPEROXIDASE (LPO)-catalyzed oxidation represents a major step in the detoxification of $H_2O_2$ which serves as the electron donor in the reaction (Sharma *et al.*, 2013). Compared with the controls, the *LPO*

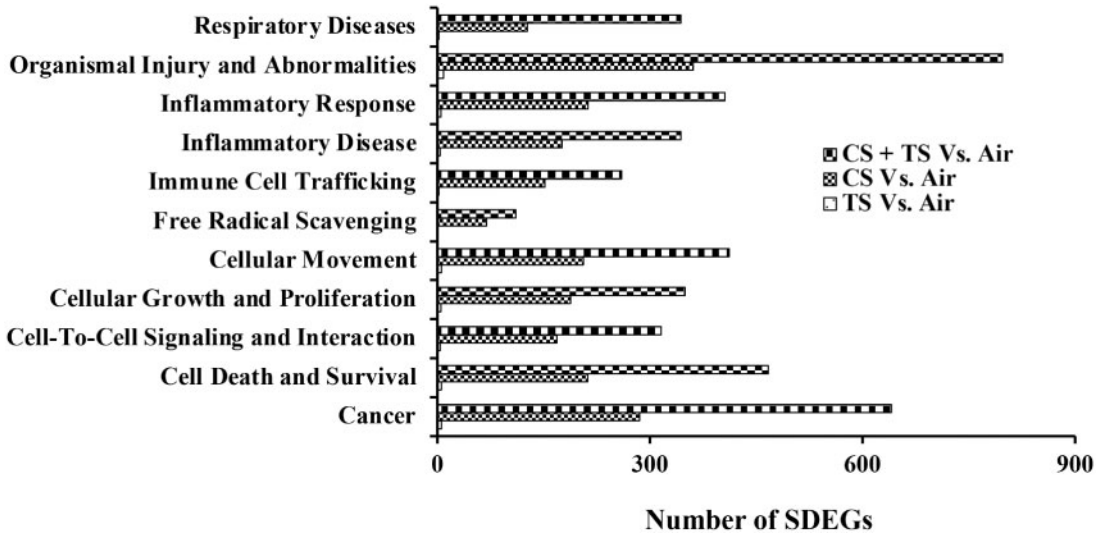


**Figure 6.** Biological functions and disease categories enriched in the lungs of the tobacco smoke (TS)-, crystalline silica (CS)-, and TS plus CS-exposed rats. Enrichment analysis of the significantly differentially expressed genes (SDEGs) detected by NGS analysis of the gene expression data was performed by Ingenuity Pathway Analysis (IPA) as described in the text. Eleven of the top-ranking-enriched biological function and disease categories, compared with the control, are presented. In the TS versus Air group of rats, the number of SDEGs belonging to the biological functions and disease categories presented ranged from 0 to 9 (please see Supplementary Table 3 for the number of SDEGs in individual categories).

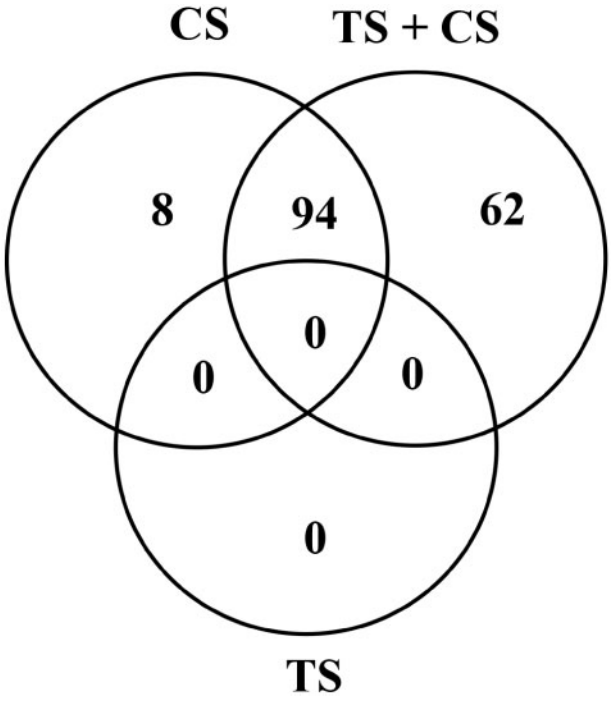


**Figure 7.** Enrichment of cancer-related biological functions in the lungs of the tobacco smoke (TS)-, crystalline silica (CS)-, and TS plus CS-exposed rats. Gene expression profiles in the lungs of the rats were determined by next generation sequencing and significantly differentially expressed genes (SDEGs) in the TS, CS, and TS + CS exposure groups, compared with the control group, were identified as described in the text. The SDEGs identified in the TS-, CS-, and TS + CS-exposed rat lungs were used as input to identify the significantly enriched ($p < .05$) cancer-related biological functions using the Ingenuity Pathway Analysis (IPA) program as described in the text. The number of unique and overlapping cancer-related biological functions significantly enriched ($p < .05$) in the lungs of the rats is presented.

transcript was 9.79-, 217.22-, and 354.13-fold overexpressed in the TS-, CS-, and CS plus TS-exposed rat lungs, respectively (Table 4), and this may represent an attempt by the exposed rat lungs to defend against the $H_2O_2$ toxicity. Despite the presumed role of *LPO* in protecting the lungs against the toxicity of $H_2O_2$, the functional significance of the *LPO* gene overexpression detected in the lungs of the exposed rats deserves further attention. This is because the *LPO*-mediated oxidation product(s) of certain substrate(s), for example, estrogens, is a risk factor for cancer (Lovstad, 2006; Sharma *et al.*, 2013). Therefore, it remains to be determined whether the *LPO* overexpression, as detected in our study, may also contribute to the carcinogenic risk associated with exposure to TS or CS—2 well known carcinogens (IARC, 1997, 2004)—as well as the exacerbation of CS-induced lung cancer by TS as previously reported (Liu *et al.*, 2013).

Activation of the mitogen-activated protein kinases (MAPKs), through the generation of ROS, has been suggested as a mechanism underlying the CS-induced lung toxicity (Ding *et al.*, 1999). The MAPKs are activated by various stimuli, including but not limited to, oxidative stress (Huang *et al.*, 2009). Bioinformatic analysis of the SDEGs detected in the current study identified the enrichment of canonical pathways involving MAPKs (Supplementary Tables 3–5). It is noteworthy that the number of significantly enriched MAPK-related canonical pathways in the lungs corresponded to the severity of toxicity induced by the agent(s). Both the number of SDEGs belonging to the MAPK-related canonical pathways and their fold changes in expression were higher in the CS plus TS-exposed lungs compared with those exposed to CS alone (Supplementary Tables 2–5). Similarly, the fold changes in expressions of several MAPK-regulated genes, for example, *DUOX1* (Ameziane-El-Hassani et al., 2015), *HMOX1* (Nakashima *et al.*, 2018), *S100A8* and *S100A9* (Kwon *et al.*, 2013), *MMP12* (Liu *et al.*, 2018), and *SPP1* (Beck and Knecht, 2003), corresponded to the severity of the lung toxicity (Figs. 1 and 2). Collectively, the correlation between the severity of lung injury and the changes in the MAPK pathways and the fold changes in expressions of the genes involved in and

**Table 4.** Fold Changes in the Expressions of Differentially Expressed Transcripts in the Lungs of the TS-, CS-, and TS + CS-Exposed Rats

| Transcript | Fold Change in Expression | | |
|---|---|---|---|
| | TS | CS | TS + CS |
| *Adenosine A1 receptor (ADORA1)* | 1.47 | 4.02 | 5.24 |
| *C-C motif chemokine ligand 2 (CCL2)* | 3.49 | 18.75 | 26.84 |
| *Chitinase, acidic (CHIA)* | 2.21 | 7.64 | 14.52 |
| *Dual oxidase 1 (DUOX1)* | 1.06 | 1.97 | 3.78 |
| *Dual oxidase maturation factor 1 (DUOXA1)* | 1.07 | 2.34 | 2.45 |
| *Estrogen receptor 1 (ESR1)* | 1.36 | 3.67 | 4.99 |
| *Heme oxygenase 1 (HMOX1)* | 1.37 | 2.74 | 3.17 |
| *Lactoperoxidase (LPO)* | 9.79 | 217.22 | 354.13 |
| *Matrix metallopeptidase 7 (MMP7)* | 1.28 | 6.01 | 7.90 |
| *Matrix metallopeptidase 12 (MMP12)* | 2.42 | 14.21 | 18.82 |
| *Matrix metallopeptidase (MMP14)* | 1.07 | 1.34 | 1.66 |
| *Matrix metallopeptidase 19 (MMP19)* | 1.07 | 1.21 | 1.57 |
| *Neutrophil cytosolic factor 1 (NCF1)* | 1.26 | 1.65 | 2.58 |
| *Neutrophil cytosolic factor 2 (NCF2)* | 1.18 | 1.84 | 2.03 |
| *Neutrophil cytosolic factor 4 (NCF4)* | 1.16 | 1.62 | 1.76 |
| *NADPH oxidase organizer 1 (NOXO1)* | 1.95 | 4.08 | 3.64 |
| *PENTRAXIN3 (PTX3)* | 2.01 | 3.46 | 5.41 |
| *Phospholipase A2 group IB (PLA2G1B)* | 1.24 | 1.83 | 2.09 |
| *Phospholipase A2, group IVE (PLA2G4E)* | 1.02 | 4,06 | 5.88 |
| *Phospholipase A2 group VII (PLA2G7)* | 1.19 | 1.88 | 2.50 |
| *Resistin like alpha (RETNLA)* | 1.23 | 15.80 | 31.34 |
| *S100 calcium-binding protein A8 (S100A8)* | 1.80 | 3.89 | 4.83 |
| *S100 calcium-binding protein A9 (S100A9)* | 2.31 | 8.87 | 9.92 |
| *S100 calcium-binding protein A10 (S100A10)* | 1.00 | 1.32 | 1.61 |
| *Solute carrier family 26 member 4 (SLC26A4)* | 4.09 | 24.15 | 30.58 |
| *Superoxide dismutase 2 (SOD2)* | 1.34 | 2.38 | 2.35 |
| *Secreted phosphoprotein 1 (SPP1)* | 2.85 | 36.69 | 72.61 |

The transcripts listed are those that are discussed in detail in the manuscript with respect to their potential role in CS-induced lung toxicity and exacerbation of the toxicity by TS. A complete list of all the transcritps detected in the rat lungs, fold changes in their expressions, and the adjusted *p* values are presented in Supplementary Table 2.

regulated by those pathways may suggest the involvement of MAPK pathways in CS-induced lung toxicity as well as the exacerbation by TS.

Inflammation plays a major role in the health effects associated with CS exposure. *Myelin-related proteins (MRPs)* play an active role in the migration of neutrophils, from blood to the site of tissue injury, resulting in an inflammatory response (Ryckman *et al.*, 2003). The transcripts of both *S100A8* and *S100A9*, 2 calcium-binding MRPs involved in neutrophil migration (Wang *et al.*, 2018), were significantly overexpressed in the lungs of all 3 groups of the exposed rats. However, the fold changes in their overexpressions were highest in the CS plus TS group, followed by the CS and the TS alone group, respectively (Table 4). The correlation in the number of neutrophils and the fold changes in the expression of *S100A8* and *S100A9* transcripts in the rat lungs, therefore, suggested their potential involvement in the CS-induced neutrophil infiltration as well as its exacerbation by the exposure to TS.

Damage/activation of AM by inhaled particles may result in the release of reactive intermediates, including those involved in an inflammatory response, potentially playing a key role in the ensuing lung pathology. Eicosanoids, a functionally diverse group of lipid mediators, are released by the AMs in response to exposure to toxic particles (Serhan, 2007). Phospholipases play a critical role in the cleavage of phospholipids to generate free fatty acids and lysophospholipids (Schaloske and Dennis, 2006). Among the phospholipases, the role of phospholipase $A_2$ ($PLA_2$) is most critical because they mediate the cleavage of phospholipids to arachidonic acid, a rate-limiting step in the synthesis of eicosanoids (Saiga *et al.*, 2005). The transcripts for 3 $PLA_2$ genes, viz, *$PLA_2g1b$*, *$PLA_2g4e$*, and *$PLA_2g7$*, were significantly overexpressed in the lungs of the CS plus TS-exposed rats. On the other hand, in the CS- and TS alone-exposed rat lungs, only 2 (*$PLA_2g4e$* and *$PLA_2g7$*) and one of the transcripts (*$PLA_2g1b$*), respectively, were significantly overexpressed. In addition, the fold changes in the overexpression of the $PLA_2$ transcripts corresponded to the severity of lung inflammation and toxicity detected in the rats. The eicosanoids generated from the $PLA_2$-meadiated cleavage of phospholipids may result in lung inflammation and toxicity by functioning as chemoattractants (Granata *et al.*, 2006). The potential role of $PLA_2$ genes in the CS-induced lung inflammation and toxicity and their exacerbation by TS is further supported by corresponding increases in the number of neutrophils infiltered into the lungs (Figure 2) and the BALF levels of several cytokines and chemokines detected in the rats (Figure 4).

Silicosis, perhaps the most serious health outcome of exposure to CS, is characterized by lung fibrosis with accompanied reduction in lung function. Degradation and rebuilding of the extracellular matrix (ECM), the key events in lung remodeling and fibrosis, are regulated by several genes. Several lines of evidence suggest a prominent role for the CCL2 gene that encodes the MCP-1 protein in fibrosis (Distler *et al.*, 2001; Ferreira *et al.*, 2006; Yamamoto and Nishioka, 2003). MATRIX METALLOPROTEINASES (MMPs), a family of proteins, play a central role in tissue remodeling by cleaving ECM and non-ECM

molecules (Page-McCaw *et al.*, 2007). The transcripts for 4 of the MMPs, viz, *MMP7*, *MMP12*, *MMP14*, and *MMP19*, were overexpressed in the exposed lungs (Table 4). *MMP12*, the most significantly overexpressed *MMP* detected in the present study, is secreted by activated AM and codes for a protein with elastolytic activity (Wagner *et al.*, 2016). The underlying mechanism responsible for the role of *MMP12* in lung damage is attributed to its proteolytic activity toward ECM, antiproteases, and proinflammatory cytokines (Churg and Wright, 2005; Hautamaki *et al.*, 1997; Zheng *et al.*, 2000). A correlation between *Chitinase (CHIA)* activity and disease severity exists in human interstitial lung diseases characterized by lung remodeling and fibrosis (Cho *et al.*, 2015; Lee *et al.*, 2012). The *Adenosine receptor A1 (ADORA1)* promotes lung ECM formation and fibrosis (Cronstein, 2011). In a murine lung fibrosis model, *Pentraxin 3 (PTX3)* facilitated the differentiation of monocytes to fibrocytes and deposition of collagen, a key component of ECM (Pilling *et al.*, 2015). In a mouse pulmonary toxicity model, *Osteopontin (SPP1)* promoted the differentiation of fibroblasts to myofibroblasts (Dong and Ma, 2017), a key event involved in lung fibrosis. The profibrotic role of 17 β-estradiol, mediated by *Estrogen receptor 1 (ESR1)*, involves an increase in collagen and the associated ECM remodeling (Aida-Yasuoka *et al.*, 2013). The increase in the abundance of all these transcripts, viz, *CCL2*, *MMP7*, *MMP12*, *MMP14*, *MMP19*, *CHIA*, *ADORA1*, *PTX3*, *SPP1*, and *ESR1*, involved in fibrosis, corresponded to the lung toxicity and fibrosis detected in the rats. These results thus suggested the contribution of the above-mentioned genes in the CS-induced lung fibrosis and toxicity as well as their exacerbations by TS.

The current study, in addition to demonstrating the involvement of oxidative stress, inflammation, and fibrosis in the lung toxicity induced by CS and its exacerbation by TS, indicated other mechanisms potentially involved in the toxicity. Enrichment of the circadian rhythm signaling pathway detected in the CS- or TS-exposed lungs was further increased in the CS plus TS-exposed lungs. The role of circadian rhythm signaling, if any, in the lung toxicity induced by CS and its exacerbation by TS have not been previously recognized despite the identification of circadian rhythm disruption in tumorigenesis (Savvidis and Koutsilieris, 2012). Calcium (Ca), due to its established role as perhaps the most pleiotropic second messenger, mediates a variety of cellular functions including those relevant to CS-induced toxicity such as signal transduction and cell growth, division, and motility (Calpham, 2007). Even though the role of Ca, if any, in CS-induced lung toxicity was not investigated in this study, several lines of evidence suggested the potential involvement of Ca in CS-induced lung toxicity and its exacerbation by TS. The *S100A8*, *S100A9*, and *S100A10* transcripts that code for prominent Ca-binding proteins were overexpressed in the lungs of the rats. Like many other transcripts, the overexpression of these Ca-binding transcripts corresponded to the pulmonary toxicity detected. A similar trend was also noticed in the enrichment of the Ca signaling and axonal guidance signaling canonical pathways in the lungs of the exposed rats (Supplementary Tables 3–5). The enrichment in the axonal guidance signaling canonical pathway, corresponding to the severity of lung toxicity detected in the rats, may suggest the potential involvement of lung neurological network through Ca-mediated modulation of axonal transport (Morotz *et al.*, 2012) in CS-induced lung toxicity and its exacerbation by TS. Despite the reported involvement of Ca in CS-induced inflammation in an *in vitro* cell culture model (Liu *et al.*, 2007), additional studies are required to determine the potential role of Ca as a second messenger in the lung response to CS exposure as well as its exacerbation by TS.

Future studies are required to validate the findings of the current study. This would include the determination of protein expression profiles to corroborate the transcriptomic changes detected in the lungs. Similarly, the functional significance of the gene expression changes needs to be determined in order to attribute a definite role for any of the differentially expressed genes in the CS-induced lung toxicity as well as its exacerbation by TS. This will involve conducting functional (toxicity) studies by employing transgenic cell culture and/or animal models of the genes or studies that involve the inhibition of protein function by employing pharmacological agent(s). In this regard, it is worth mentioning the findings of a recent study conducted in our laboratory in which the functional significance of the *Solute carrier family 26 member 4 (SLC26A4)* overexpression with respect to the CS-induced lung toxicity was investigated using transgenic mice (Sager, 2019). In the current rat study, the *SLC26A4* overexpression corresponded to the severity of lung toxicity suggesting the potential involvement of the gene in CS-induced lung toxicity as well as its exacerbation by TS. The lung response to CS exposure was significantly higher in the $SLC26A4^{+/+}$ mice compared with the $SLC26A4^{-/-}$ littermates (Sager, 2019) showing that the significant overexpression of the *SLC26A4* transcript detected in the CS-exposed rat lungs was functionally relevant to the lung toxicity as well its exacerbation by TS.

In summary, the results of the current study demonstrated a significant exacerbation of the CS-induced lung toxicity by TS in the rats. The CS-induced oxidative stress, inflammation, and fibrosis in the rat lungs were augmented by TS exposure. Bioinformatic analysis of the transcriptome data identified novel targets and molecular mechanisms potentially underlying the CS-induced lung toxicity as well as its exacerbation by TS. Further studies, especially functional genomics of the differentially expressed genes, are required to validate the findings and better understand the excess risk of coexposure to TS, an avoidable life-style factor, on the adverse health effects associated with CS exposure. This, in turn, is expected to be useful in the management and potential reduction/prevention of the adverse health effects, including silicosis and cancer, that are potentially associated with CS exposure.

## DATA AVAILABILITY

Supplementary data are available at https://doi.org/10.5061/dryad.jdfn2z38j.

## DECLARATION OF CONFLICTING INTERESTS

The authors declare no potential conflicts of interest with respect to the research, authorship, and/or publication of this article.

## FUNDING

National Institute for Occupational Safety and Health (Project Number 939050Z).

## ACKNOWLEDGMENTS

The authors thank Jared Cumpston and Brad Cumpston (NIOSH, Morgantown) for assistance with inhalation exposure of rats and Ava Winn (NIOSH, Morgantown) for analyzing the blood samples.

## REFERENCES


Aida-Yasuoka, K., Peoples, C., Yasuoka, H., Hershberger, P., Thiel, K., Cauley, J. A., Medsger, T. A., Jr, and Feghali-Bostwick, C. A. (2013). Estradiol promotes the development of a fibrotic phenotype and is increased in the serum of patients with systemic sclerosis. *Arthritis Res. Ther.* **15**, R10.

Ameziane-El-Hassani, R., Talbot, M., de Souza Dos Santos, M. C., Al Ghuzlan, A., Hartl, D., Bidart, J. M., De Deken, X., Miot, F., Diallo, I., de Vathaire, F., *et al.* (2015). NADPH oxidase DUOX1 promotes long-term persistence of oxidative stress after an exposure to irradiation. *Proc. Natl. Acad. Sci. U.S.A.* **112**, 5051–5056.

Andrews, S. (2010). *FastQC: A Quality Control Tool for High Throughput Sequence Data*. Available at: http://www.bioinformatics.babraham.ac.uk/projects/fastqc. Accessed May 21, 2019.

Anjilvel, S., and Asgharian, B. (1995). A multiple-path model of particle deposition in the rat lung. *Fundam. Appl. Toxicol.* **28**, 41–50.

Antunes, F., Han, D., and Cadenas, E. (2002). Relative contributions of heart mitochondria glutathione peroxidase and catalase to $H_2O_2$ detoxification in in vivo conditions. *Free Radic. Biol. Med.* **33**, 1260–1267.

Beck, G. R., Jr, and Knecht, N. (2003). Osteopontin regulation by inorganic phosphate is ERK1/2-, protein kinase C-, and proteasome-dependent. *J. Biol. Chem.* **278**, 41921–41929.

Bedard, K., and Krause, K. H. (2007). The NOX family of ROS-generating NADPH oxidases: Physiology and pathophysiology. *Physiol. Rev.* **87**, 245–313.

Bhalla, D. K. (1999). Ozone-induced lung inflammation and mucosal barrier disruption: Toxicology, mechanisms, and implications. *J. Toxicol. Environ. Health B Crit. Rev.* **2**, 31–86.

Bolger, A. M., Lohse, M., and Usadel, B. (2014). Trimmomatic: A flexible trimmer for Illumina sequence data. *Bioinformatics* **30**, 2114–2120.

Calpham, D. E. (2007). Calcium signaling. *Cell* **131**, 1047–1058.

Carnesecchi, S., Deffert, C., Pagano, A., Garrido-Urbani, S., Metrailler-Ruchonnet, I., Schappi, M., Donati, Y., Matthay, M. A., Krause, K. H., and Barazzone Argiroffo, C. (2009). NADPH oxidase-1 plays a crucial role in hyperoxia-induced acute lung injury in mice. *Am. J. Respir. Crit. Care Med.* **180**, 972–981.

Carter, C. A., and Misra, M. (2010). Effects of short-term cigarette smoke exposure on Fischer 344 rats and on selected lung proteins. *Toxicol. Pathol.* **38**, 402–415.

Chen, B. T., Namenyi, J., Yeh, H. C., Mauderly, J. L., and Cuddihy, R. G. (1990). Physical characterization of cigarette smoke aerosol generated from a Walton smoke machine. *Aerosol Sci. Technol.* **12**, 364–375.

Cho, S. J., Weiden, M. D., and Lee, C. G. (2015). Chitotriosidase in the pathogenesis of inflammation, interstitial lung diseases and COPD. *Allergy Asthma Immunol. Res.* **7**, 14–21.

Choi, S. J., Lee, S. H., Lee, S. J., Yang, M. J., and Lee, K. (2016). Subchronic inhalation toxicity study of 3R4F reference cigarette smoke in rats. *Mol. Cell. Toxicol.* **12**, 313–325.

Churg, A., and Wright, J. L. (2005). Proteases and emphysema. *Curr. Opin. Pulm. Med.* **11**, 153–159.

Cocco, P., Rice, C. H., Chen, J. Q., McCawley, M. A., McLaughlin, J. K., and Dosemeci, M. (2001). Lung cancer risk, silica exposure, and silicosis in Chinese mines and pottery factories: The modifying role of other workplace lung carcinogens. *Am. J. Ind. Med.* **40**, 674–682.

Cohen, D., Arai, S. F., and Brain, J. D. (1979). Smoking impairs long-term dust clearance from the lung. *Science* **204**, 514–517.

Cronstein, B. N. (2011). Adenosine receptors and fibrosis: A translational review. *F1000 Biol. Rep.* **3**, 21.

Ding, M., Shi, X., Dong, Z., Chen, F., Lu, Y., Castranova, V., and Vallyathan, V. (1999). Freshly fractured crystalline silica induces activator protein-1 activation through ERKs and p38 MAPK. *J. Biol. Chem.* **274**, 30611–30616.

Distler, O., Pap, T., Kowal-Bielecka, O., Meyringer, R., Guiducci, S., Landthaler, M., Scholmerich, J., Michel, B. A., Gay, R. E., Matucci-Cerinic, M., *et al.* (2001). Overexpression of monocyte chemoattractant protein 1 in systemic sclerosis: Role of platelet-derived growth factor and effects on monocyte chemotaxis and collagen synthesis. *Arthritis Rheum.* **44**, 2665–2678.

Doney, B. C., Miller, W. E., Hale, J. M., and Syamlal, G. (2020). Estimation of the number of workers exposed to respirable crystalline silica by industry: Analysis of OSHA compliance data (1979–2015). *Am. J. Ind. Med.* **63**, 465–477.

Dong, J., and Ma, Q. (2017). Osteopontin enhances multi-walled carbon nanotube-triggered lung fibrosis by promoting TGF-beta1 activation and myofibroblast differentiation. *Part. Fibre Toxicol.* **14**, 18.

Dorman, D. C., Mokashi, V., Wagner, D. J., Olabisi, A. O., Wong, B. A., Moss, O. R., Centeno, J. A., Guandalini, G., Jackson, D. A., Dennis, W. E., *et al.* (2012). Biological responses in rats exposed to cigarette smoke and Middle East sand (dust). *Inhal. Toxicol.* **24**, 109–124.

Ferreira, A. M., Takagawa, S., Fresco, R., Zhu, X., Varga, J., and DiPietro, L. A. (2006). Diminished induction of skin fibrosis in mice with MCP-1 deficiency. *J. Invest. Dermatol.* **126**, 1900–1908.

Gehr, P., Bachofen, M., and Weibel, E. R. (1978). The normal human lung: Ultrastructure and morphometric estimation of diffusion capacity. *Respir. Physiol.* **32**, 121–140.

Granata, F., Frattini, A., Loffredo, S., Del Prete, A., Sozzani, S., Marone, G., and Triggiani, M. (2006). Signaling events involved in cytokine and chemokine production induced by secretory phospholipase A2 in human lung macrophages. *Eur. J. Immunol.* **36**, 1938–1950.

Greenberg, M. I., Waksman, J., and Curtis, J. (2007). Silicosis: A review. *Dis. Mon.* **53**, 394–416.

Hautamaki, R. D., Kobayashi, D. K., Senior, R. M., and Shapiro, S. D. (1997). Requirement for macrophage elastase for cigarette smoke-induced emphysema in mice. *Science* **277**, 2002–2004.

Hessel, P. A., Gamble, J. F., and Nicolich, M. (2003). Relationship between silicosis and smoking. *Scand. J. Work Environ. Health* **29**, 329–336.

Huang, G., Shi, L. Z., and Chi, H. (2009). Regulation of JNK and p38 MAPK in the immune system: Signal integration, propagation and termination. *Cytokine* **48**, 161–169.

IARC. (1997). Silica, some silicates, coal dust and para-aramid fibrils. International Agency for Research on Cancer, Lyon, France. *IARC Monogr. Eval. Carcinog. Risks Hum.* **68**, 1–242.

IARC. (2004). Tobacco smoke and involuntary smoking. International Agency for Research on Cancer, Lyon, France. *IARC Monogr. Eval. Carcinog. Risks Hum. Tobacco Smoke and Involuntary Smoking* **83**, 1–1473.

Jacob, C. O., Eisenstein, M., Dinauer, M. C., Ming, W., Liu, Q., John, S., Quismorio, F. P., Jr, Reiff, A., Myones, B. L., Kaufman, K. M., *et al.* (2012). Lupus-associated causal mutation in neutrophil cytosolic factor 2 (NCF2) brings unique insights to the structure and function of NADPH oxidase. *Proc. Natl. Acad. Sci. U.S.A.* **109**, E59–E67.

Kim, D., Langmead, B., and Salzberg, S. L. (2015). HISAT: A fast spliced aligner with low memory requirements. *Nat. Methods* **12**, 357–360.

Kwon, C. H., Moon, H. J., Park, H. J., Choi, J. H., and Park, D. Y. (2013). S100A8 and S100A9 promotes invasion and migration through p38 mitogen-activated protein kinase-dependent NF-kappaB activation in gastric cancer cells. *Mol. Cells* **35**, 226–234.

Law, C. W., Alhamdoosh, M., Su, S., Dong, X., Tian, L., Smyth, G. K., and Ritchie, M. E. (2016). RNA-seq analysis is easy as 1-2-3 with limma, Glimma and edgeR. *F1000Research* **5**, 1408–1429.

Lee, C. G., Herzog, E. L., Ahangari, F., Zhou, Y., Gulati, M., Lee, C. M., Peng, X., Feghali-Bostwick, C., Jimenez, S. A., Varga, J., *et al.* (2012). Chitinase 1 is a biomarker for and therapeutic target in scleroderma-associated interstitial lung disease that augments TGF-beta1 signaling. *J. Immunol.* **189**, 2635–2644.

Li, H., Handsaker, B., Wysoker, A., Fennell, T., Ruan, J., Homer, N., Marth, G., Abecasis, G., and Durbin, R; 1000 Genome Project Data Processing Subgroup. (2009). The Sequence Alignment/Map format and SAMtools. *Bioinformatics* **25**, 2078–2079.

Liu, C., Zhang, C., Jia, L., Chen, B., Liu, L., Sun, J., Zhang, W., You, B., Li, Y., Li, P., *et al.* (2018). Interleukin-3 stimulates matrix metalloproteinase 12 production from macrophages promoting thoracic aortic aneurysm/dissection. *Clin. Sci. (Lond).* **132**, 655–668.

Liu, H., Zhang, H., and Forman, H. J. (2007). Silica induces macrophage cytokines through phosphatidylcholine-specific phospholipase C with hydrogen peroxide. *Am. J. Respir. Cell Mol. Biol.* **36**, 594–599.

Liu, Y., Steenland, K., Rong, Y., Hnizdo, E., Huang, X., Zhang, H., Shi, T., Sun, Y., Wu, T., and Chen, W. (2013). Exposure-response analysis and risk assessment for lung cancer in relationship to silica exposure: A 44-year cohort study of 34,018 workers. *Am. J. Epidemiol.* **178**, 1424–1433.

Lovstad, R. A. (2006). A kinetic study on the lactoperoxidase catalyzed oxidation of estrogens. *Biometals* **19**, 587–592.

Morotz, G. M., De Vos, K. J., Vagnoni, A., Ackerley, S., Shaw, C. E., and Miller, C. C. (2012). Amyotrophic lateral sclerosis-associated mutant VAPBP56S perturbs calcium homeostasis to disrupt axonal transport of mitochondria. *Hum. Mol. Genet.* **21**, 1979–1988.

Nakashima, K., Sato, T., Shigemori, S., Shimosato, T., Shinkai, M., and Kaneko, T. (2018). Regulatory role of heme oxygenase-1 in silica-induced lung injury. *Respir. Res.* **19**, 144.

National Institute for Occupational Safety and Health. (1976). A *Guide to Industrial Respiratory Protection*, by J.A. Pritchard (DHEW/PHS/CDC/NIOSH Pub. No. 76-189). Available at: https://www.cdc.gov/niosh/nioshtic-2/00058285.html. Accessed May 25, 2020.

National Institute for Occupational Safety and Health. (1996). *Preventing Silicosis and Deaths in Construction Workers*. DHHS (NIOSH) Publication Number 96-112. Available at: https://www.cdc.gov/niosh/docs/96-112/default.html. Accessed May 25, 2020.

Occupational Safety and Health Administration. (2013). *OSHA'a Proposed Crystalline Silica Rule: Overview. OSHA Factsheet*. Available at: https://www.osha.gov/silica/factsheets/OSHA_FS-3683_Silica_Overview.pdf. Accessed May 25, 2020.

Ohashi, T., Pinkerton, K., Ikegami, M., and Jobe, A. H. (1994). Changes in alveolar surface area, surfactant protein A, and saturated phosphatidylcholine with postnatal rat lung growth. *Pediatr. Res.* **35**, 685–689.

Page-McCaw, A., Ewald, A. J., and Werb, Z. (2007). Matrix metalloproteinases and the regulation of tissue remodelling. *Nat. Rev. Mol. Cell Biol.* **8**, 221–233.

Pilling, D., Cox, N., Vakil, V., Verbeek, J. S., and Gomer, R. H. (2015). The long pentraxin PTX3 promotes fibrocyte differentiation. *PLoS One* **10**, e0119709.

Qu, Y., Tang, Y., Cao, D., Wu, F., Liu, J., Lu, G., Zhang, Z., and Xia, Z. (2007). Genetic polymorphisms in alveolar macrophage response-related genes, and risk of silicosis and pulmonary tuberculosis in Chinese iron miners. *Int. J. Hyg. Environ. Health* **210**, 679–689.

R Core Team. (2018). *R: A Language and Environment for Statistical Computing*. R Foundation for Statistical Computing, Vienna, Austria. Available at: http://www.R-project.org/. Accessed May 21, 2019.

Roberts, J. R., Anderson, S. E., Kan, H., Krajnak, K., Thompson, J. A., Kenyon, A., Goldsmith, W. T., McKinney, W., Frazer, D. G., Jackson, M., *et al.* (2014). Evaluation of pulmonary and systemic toxicity of oil dispersant (COREXIT EC9500A((R))) following acute repeated inhalation exposure. *Environ. Health Insights* **8**, 63–74.

Roemer, E. S. H., Weiler, H., Buettner, A., Kausche, S., Weber, S., Berges, A., Stueber, M., Muench, M., Trelles-Sticken, E., Pype, J., *et al.* (2012). Mainstream smoke chemistry and *in vitro* and *in vivo* toxicity of the reference cigarettes 3R4F and 2R4F. *Contrib. Tobacco Res.* **25**, 316–335.

Ryckman, C., McColl, S. R., Vandal, K., de Medicis, R., Lussier, A., Poubelle, P. E., and Tessier, P. A. (2003). Role of S100A8 and S100A9 in neutrophil recruitment in response to monosodium urate monohydrate crystals in the air-pouch model of acute gouty arthritis. *Arthritis Rheum.* **48**, 2310–2320.

Sager, T. (2019). Functional significance of the SLC26A4 gene in silica-induced pulmonary toxicity. *Toxicol. Suppl Toxicol. Sci.* **168**, Abstract No. 2017.

Saiga, A., Uozumi, N., Ono, T., Seno, K., Ishimoto, Y., Arita, H., Shimizu, T., and Hanasaki, K. (2005). Group X secretory phospholipase A2 can induce arachidonic acid release and eicosanoid production without activation of cytosolic phospholipase A2 alpha. *Prostaglandins Other Lipid Mediat.* **75**, 79–89.

Sato, T., Shimosato, T., Alvord, W. G., and Klinman, D. M. (2008). Suppressive oligodeoxynucleotides inhibit silica-induced pulmonary inflammation. *J. Immunol.* **180**, 7648–7654.

Sato, T., Shimosato, T., and Klinman, D. M. (2018). Silicosis and lung cancer: Current perspectives. *Lung Cancer (Auckl).* **9**, 91–101.

Savvidis, C., and Koutsilieris, M. (2012). Circadian rhythm disruption in cancer biology. *Mol. Med.* **18**, 1249–1260.

Schaller, J. P., Keller, D., Poget, L., Pratte, P., Kaelin, E., McHugh, D., Cudazzo, G., Smart, D., Tricker, A. R., Gautier, L., *et al.* (2016). Evaluation of the tobacco heating system 2.2. Part 2: Chemical composition, genotoxicity, cytotoxicity, and physical properties of the aerosol. *Regul. Toxicol. Pharmacol.* **81**, S27–S47.

Schaloske, R. H., and Dennis, E. A. (2006). The phospholipase A2 superfamily and its group numbering system. *Biochim. Biophys. Acta* **1761**, 1246–1259.

Sellamuthu, R., Umbright, C., Roberts, J. R., Chapman, R., Young, S. H., Richardson, D., Leonard, H., McKinney, W., Chen, B., Frazer, D., *et al.* (2011). Blood gene expression profiling detects silica exposure and toxicity. *Toxicol. Sci.* **122**, 253–264.

Sellamuthu, R., Umbright, C., Roberts, J. R., Cumpston, A., McKinney, W., Chen, B. T., Frazer, D., Li, S., Kashon, M., and Joseph, P. (2013). Molecular insights into the progression of

crystalline silica-induced pulmonary toxicity in rats. *J. Appl. Toxicol.* **33**, 301–312.

Serhan, C. N. (2007). Resolution phase of inflammation: Novel endogenous anti-inflammatory and proresolving lipid mediators and pathways. *Annu. Rev. Immunol.* **25**, 101–137.

Sharma, S., Singh, A. K., Kaushik, S., Sinha, M., Singh, R. P., Sharma, P., Sirohi, H., Kaur, P., and Singh, T. P. (2013). Lactoperoxidase: Structural insights into the function, ligand binding and inhibition. *Int. J. Biochem. Mol. Biol.* **4**, 108–128.

Tse, L. A., Yu, I. T., Qiu, H., and Leung, C. C. (2014). Joint effects of smoking and silicosis on diseases to the lungs. *PLoS One* **9**, e104494.

U.S. Department of Health and Human Services. (2008). Centers for Disease Control and Prevention. National Institute for Occupational Safety and Health. Work-Related Lung Disease Surveillance System (eWoRLD). Silicosis. Available at https://wwwn.cdc.gov/eWorld/Grouping/Silicosis/94. Accessed May 25, 2020.

U.S. Department of Health and Human Services (USDHHS). (2014). *The Health Consequences of Smoking—50 Years of Progress. A Report of the Surgeon General Executive Summary*. U.S. Department of Health and Human Services, Centers for Disease Control and Prevention, National Center for Chronic Disease Prevention and Health Promotion, Office on Smoking and Health. pp. 1–22.

Wagner, C. J., Schultz, C., and Mall, M. A. (2016). Neutrophil elastase and matrix metalloproteinase 12 in cystic fibrosis lung disease. *Mol. Cell. Pediatr.* **3**, 25.

Wang, S., Song, R., Wang, Z., Jing, Z., Wang, S., and Ma, J. (2018). S100A8/A9 in inflammation. *Front. Immunol.* **9**, 1298.

Wu, F., Qu, Y., Tang, Y., Cao, D., Sun, P., and Xia, Z. (2008). Lack of association between cytokine gene polymorphisms and silicosis and pulmonary tuberculosis in Chinese iron miners. *J. Occup. Health* **50**, 445–454.

Xu, X., Bishop, E. E., Kennedy, S. M., Simpson, S. A., and Pechacek, T. F. (2015). Annual healthcare spending attributable to cigarette smoking: An update. *Am. J. Prev. Med.* **48**, 326–333.

Yamamoto, T., and Nishioka, K. (2003). Role of monocyte chemoattractant protein-1 and its receptor, CCR-2, in the pathogenesis of bleomycin-induced scleroderma. *J. Invest. Dermatol.* **121**, 510–516.

Yucesoy, B., Vallyathan, V., Landsittel, D. P., Sharp, D. S., Weston, A., Burleson, G. R., Simeonova, P., McKinstry, M., and Luster, M. I. (2001). Association of tumor necrosis factor-alpha and interleukin-1 gene polymorphisms with silicosis. *Toxicol. Appl. Pharmacol.* **172**, 75–82.

Zhang, M., Peng, L. L., Ji, X. L., Yang, H. B., Zha, R. S., and Gui, G. P. (2019). Tumor necrosis factor gene polymorphisms are associated with silicosis: A systemic review and meta-analysis. *Biosci. Rep.* **39**, 1–10.

Zheng, T., Zhu, Z., Wang, Z., Homer, R. J., Ma, B., Riese, R. J., Jr, Chapman, H. A., Jr, Shapiro, S. D., and Elias, J. A. (2000). Inducible targeting of IL-13 to the adult lung causes matrix metalloproteinase- and cathepsin-dependent emphysema. *J. Clin. Invest.* **106**, 1081–1093.